



## Improvement of carbothermic reduction of nickel slag by addition of $\text{CaCO}_3$

Xiao-ming LI<sup>1,2</sup>, Zhen-yu WEN<sup>1</sup>, Yi LI<sup>1</sup>, Hai-bo YANG<sup>1</sup>, Xiang-dong XING<sup>1,2</sup>

1. School of Metallurgical Engineering, Xi'an University of Architecture and Technology, Xi'an 710055, China;

2. Shaanxi Engineering Research Center of Metallurgy,

Xi'an University of Architecture and Technology, Xi'an 710055, China

Received 25 February 2019; accepted 28 October 2019

**Abstract:** The effect of  $\text{CaCO}_3$  addition on the carbothermic reduction of nickel slag was studied, and the mechanism of  $\text{CaCO}_3$  in improving the reduction was analyzed. The results showed that when the  $\text{CaCO}_3$  content added to the slag was increased from 0 to 8 wt.%, initiation temperature of the carbothermic reaction decreased from 1100 to 1000 °C, the temperature reaching the maximum reduction rate decreased from 1150 to 1100 °C, and the reduction degree of the nickel slag increased from 58% to 88%. The iron particles in the reduced nickel slag were coarsened and the X-ray diffraction intensity of metallic iron peaks increased, confirming that the addition of  $\text{CaCO}_3$  was beneficial to the reduction of nickel slag and recovery of iron.

**Key words:** nickel slag; fayalite; carbothermic reduction;  $\text{CaCO}_3$

### 1 Introduction

Rapid development of the iron and steel industry has increased the demand for iron sources. Nickel slag, a by-product of nickel flash-smelting and oxygen-enriched top-blowing processes [1], contains a high iron content and different quantities of valuable metals, such as nickel, copper, cobalt, gold, and silver [2]. It is a potential resource for the iron and steel industry. About 40 million tons of nickel slag has accumulated in China and about two million tons of new nickel slags are manufactured each year [3]. Most of this slag remains stockpiled, which occupies land and wastes metal resources. Development and utilization of nickel slag can meet the requirement for comprehensive utilization of secondary resources, with its associated environmental, economic, and social benefits.

Many processes for utilization of nickel slag have been developed in the past few decades. The processes are classified into three categories: extraction of valuable metal elements by leaching processes, preparation of ferroalloys, corrosion-resistant steel or nickel matte by smelting reduction, and production of concentrated iron powder by direct reduction followed by magnetic

separation. In the leaching processes, iron enters the tailings for further processing and produces secondary pollution, such as waste acid, waste water, and residue containing heavy metal ions. In the smelting reduction process, iron is primarily present in nickel slag in the form of silicates, so it is difficult to reduce, separate and concentrate, and it is necessary to raise the slag smelting temperature, which leads to high energy consumption, a large amount of secondary residue, and strict production control conditions. The direct reduction process is generally preferred because of its low smelting temperature and stable processing technology [4–6]. Nickel slag is difficult to reduce because of its complex mineral composition, so improving its reduction to enable extraction of valuable metal elements has become an urgent issue.

There have been many advances in the reduction of iron-containing materials. Addition of  $\text{Na}_2\text{CO}_3$  promoted the carbothermic reduction of high-phosphorus limonite and siderite ores [7,8]. Increased  $\text{CaCO}_3$  content was shown to be beneficial to the direct reduction and melting of a low-alkalinity vanadium–titanomagnetite concentrate [9]. The metallurgical properties of a titanium-bearing blast-furnace slag were improved by adding CaO [10,11]. A small amount of  $\text{Na}_2\text{CO}_3$  was

beneficial to the reduction of iron oxide during a redox process and increased its reduction degree [12,13]. Although many experiments have been performed to promote the reduction process with additives, the enhanced reduction of nickel slag has not been systematically studied.

In this work, the mechanism of the improved reduction with  $\text{CaCO}_3$  during carbothermic reduction of nickel slag was investigated. The effects of reduction conditions on the carbothermic reduction of the slag, including reduction temperature and  $\text{CaCO}_3$  content, were studied. The method proposed in this work provides a good technical and theoretical basis for comprehensive utilization of nickel slag and other similar smelting slags.

## 2 Experimental

### 2.1 Raw materials

The nickel slag was a by-product of nickel smelting in a flash furnace, and it was collected from a plant in China. The chemical composition of the nickel slag is given in Table 1. The contents of total Fe,  $\text{SiO}_2$ , and CaO were 39.40%, 32.80%, and 1.20%, respectively. X-ray diffraction (XRD), shown in Fig. 1, confirmed that the main phases of the nickel slag were  $\text{Fe}_2\text{SiO}_4$  and  $\text{Mg}_2\text{SiO}_4$ . The slag was ground to a size less than 0.074 mm before use in experiments. High-purity graphite powder was used as the reducing agent, and  $\text{CaCO}_3$  was used to promote the reaction.

**Table 1** Chemical composition of nickel slag (wt.%)

TFe	FeO	$\text{SiO}_2$	MgO	CaO	Ni	Cu	Co	S
39.40	50.66	32.50	9.70	1.20	0.455	0.338	0.144	0.868

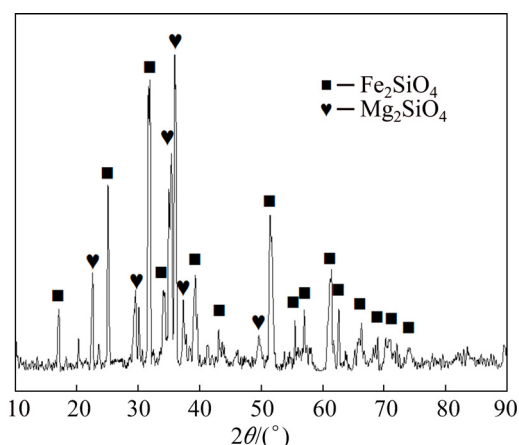


**Fig. 1** X-ray diffraction pattern of nickel slag

Scanning electron microscopy–energy dispersive spectroscopy (SEM–EDS) analysis results of the nickel slag is shown in Fig. 2. The EDS analysis showed that the slag was primarily composed of Fe, O, Si, Mg and S.

The O and Si formed  $\text{SiO}_2$  that was uniformly distributed in the slag. Fe was primarily distributed in the gaps among large particles. The large particles were mainly solid solutions formed by Mg and silicate. S existed in the slag in the form of small particles, indicating that the sulfide and silicate did not form a solid solution.

### 2.2 Experiment

Thermogravimetry (TG), which provides a direct measurement of mass loss during a reaction as a function of time, is an effective technique to study the reaction processes. TG (SETARAM SETSYS Evolution, France) was used to study the carbothermic reduction of the nickel slag. Approximately 5 mg of sample was used for each experiment, placed in a circular crucible with a height of 8 mm and a diameter of 5 mm. The mass loss of the sample was recorded from room temperature to 1200 °C at a heating rate of 20 °C/min. To ensure the reproducibility of the results, each test was repeated three times.

Reduction experiments were performed in a vertical high-temperature tube furnace. A schematic of the experimental apparatus is shown in Fig. 3. The main section of the apparatus was a vertical tube furnace equipped with an automatic balance that had a detection precision of 1 mg. The temperature of the furnace was controlled by a temperature controller. The accuracy of the temperature measurement was  $\pm 1$  K. The balance and temperature controller were connected to a computer that was used to collect the experimental data. Argon gas (99.999% in purity) was used as a shielding gas [14].

To ensure complete reaction of the sample, the ratio of the actual carbon content added to the theoretical carbon required was 1.2:1 (i.e., 20% stoichiometric excess). The nickel slag was uniformly mixed with the graphite powder and  $\text{CaCO}_3$ , and then pressed into a cylinder with diameter of 8 mm and mass of about 5 g. Polyvinyl alcohol (2 wt.%) was used as a binder. The briquette was placed in a corundum crucible, which was placed into the furnace under a flowing argon atmosphere (0.8 L/min) and heated. When the temperature of non-isothermal carbothermic reduction reached the set value (600, 800, 1000, 1100 and 1200 °C), the crucible was quickly removed and cooled in an argon atmosphere (0.8 L/min). The reduced nickel slag was crushed and milled to less than 0.074 mm to determine the phase composition and morphology.

The crystalline phases of the raw material and reduced samples were identified by XRD (PANalytical, Netherlands) using  $\text{Cu K}_\alpha$  radiation at 40 kV and 40 mA, and a scan speed of 4 (°)/min with a step of 0.026°. The morphology of the samples was characterized by SEM (Phenom-World, Netherlands) equipped with an EDS using an acceleration voltage of 15 kV.

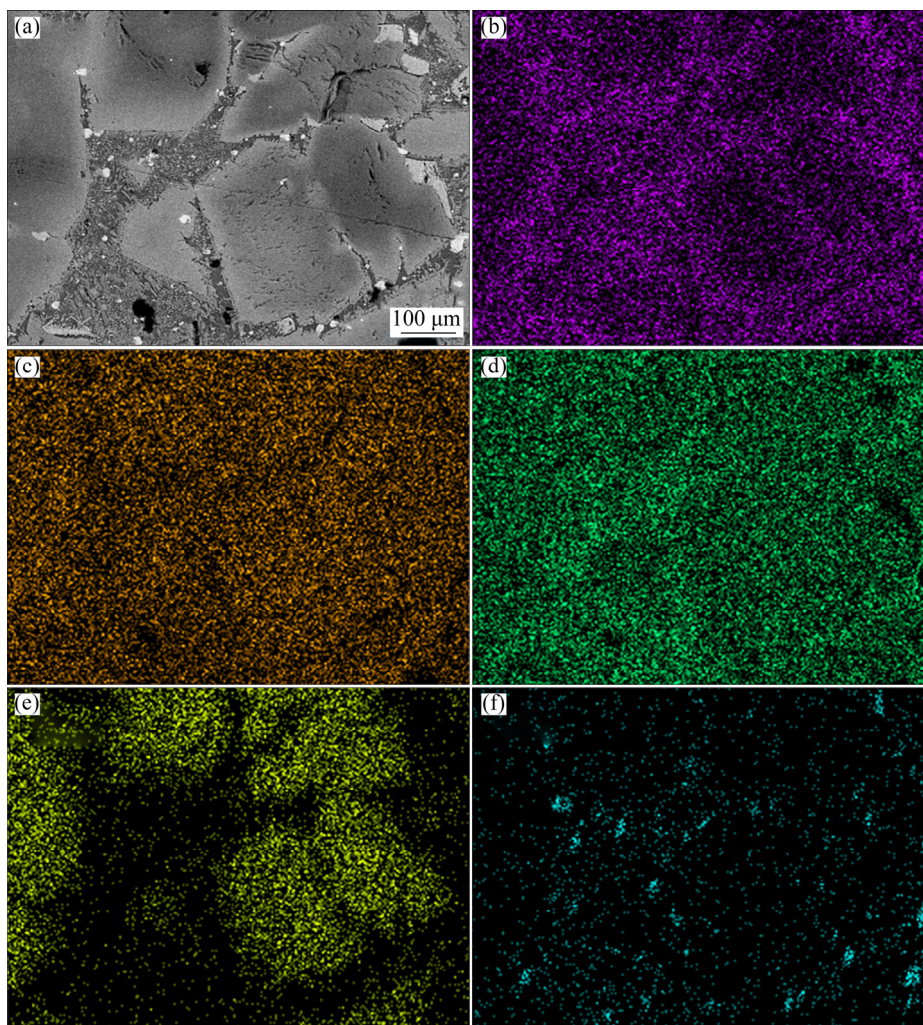


**Fig. 2** Scanning electron micrographs and energy-dispersive spectra of nickel slag: (a) Image of nickel slag; (b) Distribution of Fe; (c) Distribution of O; (d) Distribution of Si; (e) Distribution of Mg; (f) Distribution of S

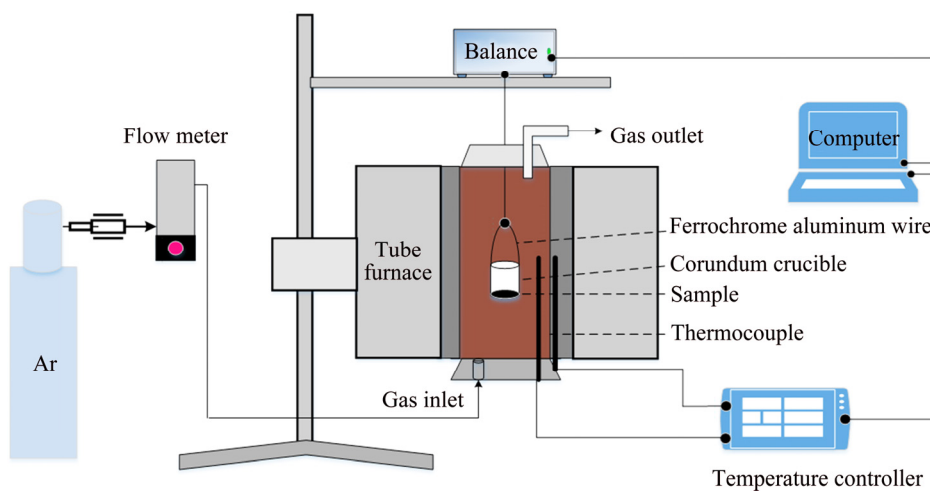


**Fig. 3** Schematic of experimental apparatus

### 2.3 Determination of reduction degree

Reduction of oxide in the nickel slag caused a mass loss because oxygen in the crystal structure of oxide is released during the reduction process. The reduction

degree ( $\alpha$ ) of the nickel slag at any time  $t$  is defined as the ratio of the loss of gas in an experiment to the theoretical maximum gas loss:

$$\alpha = (\Delta m_t / m_0) \times 100\% \quad (1)$$

where  $\Delta m_t$  is the mass loss of gas at reduction time  $t$ , and  $m_0$  is the theoretical mass loss.

## 2.4 Thermodynamic calculations

Thermodynamics of the reactions between carbon and the main components in the nickel slag were calculated by FactSage software. The basic principle is to minimize the Gibbs free energy of the constant-temperature and constant-pressure system by satisfying the material balance equation. The calculated temperatures were 25–1200 °C and the pressure of the system was 101.325 kPa. The main reaction and Gibbs free energy changes are given in Table 2 [15]. The calculated amounts of substances at different temperatures are shown in Fig. 4.

**Table 2** Main reactions and standard Gibbs free energies

No.	Equation	$\Delta G^\ominus / (\text{J} \cdot \text{mol}^{-1})$	$T_{\text{start}} / ^\circ\text{C}$
(2)	$\text{C}(\text{s}) + \text{CO}_2(\text{g}) = 2\text{CO}(\text{g})$	$123849.35 - 176.16T$	429.90
(3)	$\text{FeO}(\text{s}) + \text{C}(\text{s}) = \text{Fe}(\text{s}) + \text{CO}(\text{g})$	$111619.7 - 154.95T$	447.21
(4)	$\text{Fe}_2\text{SiO}_4(\text{s}) + 2\text{C}(\text{s}) = 2\text{Fe}(\text{s}) + \text{SiO}_2(\text{s}) + 2\text{CO}(\text{g})$	$319421.16 - 299.85T$	792.12
(5)	$\text{CaO}(\text{s}) + \text{Fe}_2\text{SiO}_4(\text{s}) + 2\text{C}(\text{s}) = \text{CaSiO}_3(\text{s}) + 2\text{Fe}(\text{s}) + 2\text{CO}(\text{g})$	$241859 - 317.94T$	487.56

Table 2 shows that  $\text{CO}_2$  which was dissociated from  $\text{CaCO}_3$  underwent a Boudouard reaction with C, which promoted the carbon gasification reaction and increased the CO content of the gaseous reducing agent. Mass and heat transfer during the reducing reaction can be optimized by  $\text{CO}_2$  [16,17]. The Gibbs free energy change of Eq. (5) was significantly lower than that of Eq. (4), indicating that the former was more likely to occur. CaO which was dissociated from  $\text{CaCO}_3$  could replace FeO in fayalite, which could increase the reducing activity of FeO and promote the reduction of nickel slag [18].

The initial reactants of nickel slag contained 0.5 mol FeO, 0.5 mol  $\text{Fe}_2\text{SiO}_4$  and 1.2 mol C, and the initial reactants of nickel slag with 8 wt.%  $\text{CaCO}_3$  (Fig. 4(b)) contained 0.5 mol FeO, 0.5 mol  $\text{Fe}_2\text{SiO}_4$ , 1.2 mol C and 0.17 mol  $\text{CaCO}_3$ . By comparing Fig. 4(a) with 4(b), the addition of  $\text{CaCO}_3$  caused changes in the amount and composition of substances in carbothermic reduction products of nickel slag at different temperatures. In the equilibrium compositions with  $\text{CaCO}_3$  addition (Fig. 4(b)), the content of iron in the reduction product was significantly higher than that without adding  $\text{CaCO}_3$  (Fig. 4(a)). In addition,  $\text{CaSiO}_3$  appeared in the slag, while the content of  $\text{Fe}_2\text{SiO}_4$  decreased and the content of FeO increased. The results showed that CaO, the

decomposition product of added  $\text{CaSiO}_3$ , reacted with  $\text{Fe}_2\text{SiO}_4$  to form  $\text{CaSiO}_3$ , and FeO was dissociated and then was further reduced to iron. The thermodynamic calculation diagram clearly showed that the addition of  $\text{CaCO}_3$  can promote the carbothermic reduction of nickel slag.

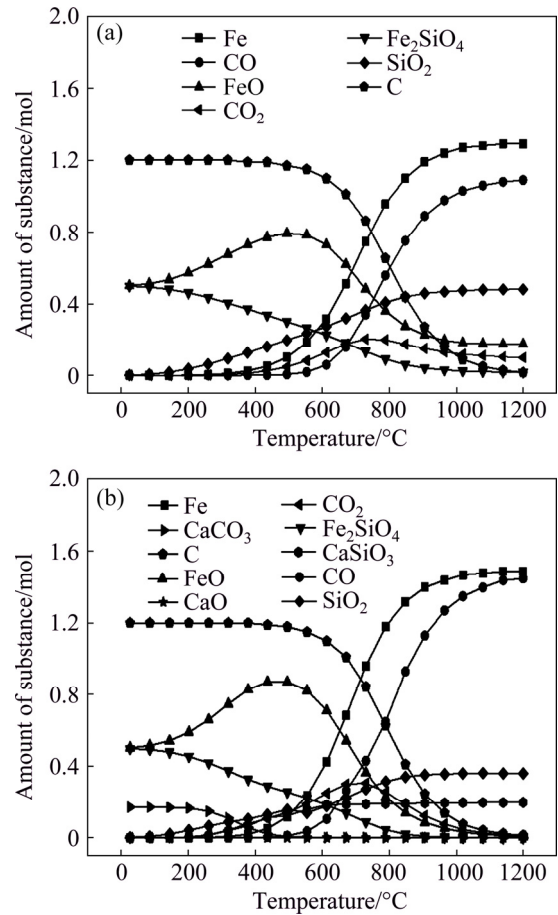


**Fig. 4** Calculated amounts of substances at different temperatures: (a) Without adding  $\text{CaCO}_3$ ; (b) With 8 wt.%  $\text{CaCO}_3$

## 3 Results and discussion

### 3.1 Effect of $\text{CaCO}_3$ content on reduction degree

The effect of  $\text{CaCO}_3$  content on the degree of iron reduction in the nickel slag at a heating rate of 20 °C/min is shown in Fig. 5. The amount of  $\text{CaCO}_3$  added had a significant effect. At a given reduction temperature and time, the reduction degree of the iron increased with increasing  $\text{CaCO}_3$  content of the raw material. The longer the reduction time, the more obvious the trend was.

After 90 min reduction, the reduction degree of the iron in the samples without adding  $\text{CaCO}_3$  was 58%; this value was increased to 70%, 80%, 85% and 88% when the  $\text{CaCO}_3$  added contents were 2, 4, 6 and 8 wt.%, respectively. The reduction degrees of the iron were

increased by 12%, 22%, 27% and 30%, respectively. It was indicated that  $\text{CaCO}_3$  had a positive effect of  $\text{CaCO}_3$  on the reduction of nickel slag as the  $\text{CaCO}_3$  content was increased from 0 to 8 wt.%.

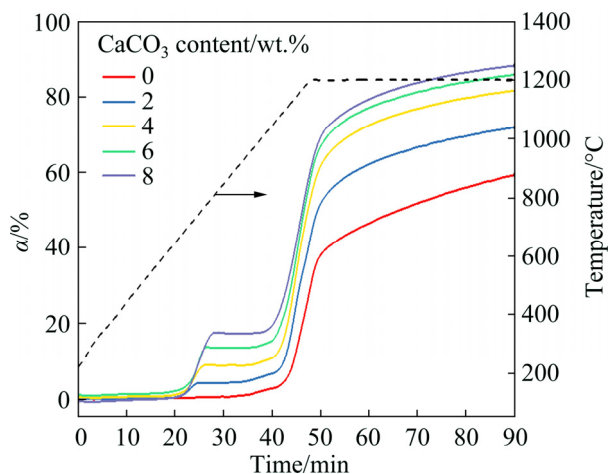


**Fig. 5** Effect of  $\text{CaCO}_3$  content on reduction degree

The effects of reduction temperature and  $\text{CaCO}_3$  content on the reaction rate are shown in Fig. 6. The reaction rate remained unchanged at temperatures below 600 °C. As the temperature was increased, the reaction rate increased. The reaction rate reached the maximum rate of reduction between 1100 and 1150 °C. As the ferrous oxide content in the slag and consumption of graphite decreased, the reaction rate decreased.

The reaction rate increased with the addition of  $\text{CaCO}_3$ . When the temperature reached 1000 °C, the reduction of ferrous oxide in the raw material was initiated. The reaction rate of the sample with adding  $\text{CaCO}_3$  was significantly higher than that without adding  $\text{CaCO}_3$ , indicating that the presence of  $\text{CaCO}_3$  could increase the reaction rate and promote the reduction of

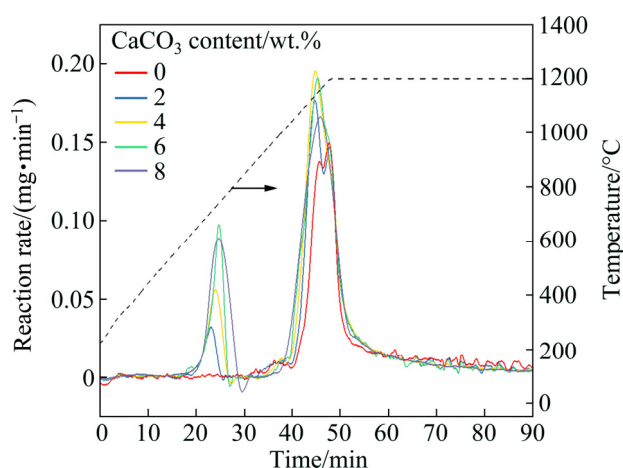


**Fig. 6** Effects of reduction temperature and  $\text{CaCO}_3$  content on reaction rate

iron in the nickel slag. The reaction reached its peak rate within 40–50 min. The reaction rate of the sample without adding  $\text{CaCO}_3$  was 0.143 mg/min; when the  $\text{CaCO}_3$  additions were 2, 4, 6 and 8 wt.%, the reaction rates were 0.168, 0.191, 0.189 and 0.177 mg/min, respectively. The peak reaction rate occurred at an earlier time for samples with adding  $\text{CaCO}_3$  and the peak reaction temperature was lower. Addition of  $\text{CaCO}_3$  reduced both the time and temperature required for the reduction rate to reach its peak value.

The optimal parameters for nickel slag reduction were 8 wt.%  $\text{CaCO}_3$  added, a reduction temperature of 1200 °C, and a retention time of 45 min.

## 3.2 Characteristics of reduced nickel slag

### 3.2.1 Effect of $\text{CaCO}_3$ content

SEM images of nickel slag added with different contents of  $\text{CaCO}_3$  reduced at 1100 °C are shown in Fig. 7.

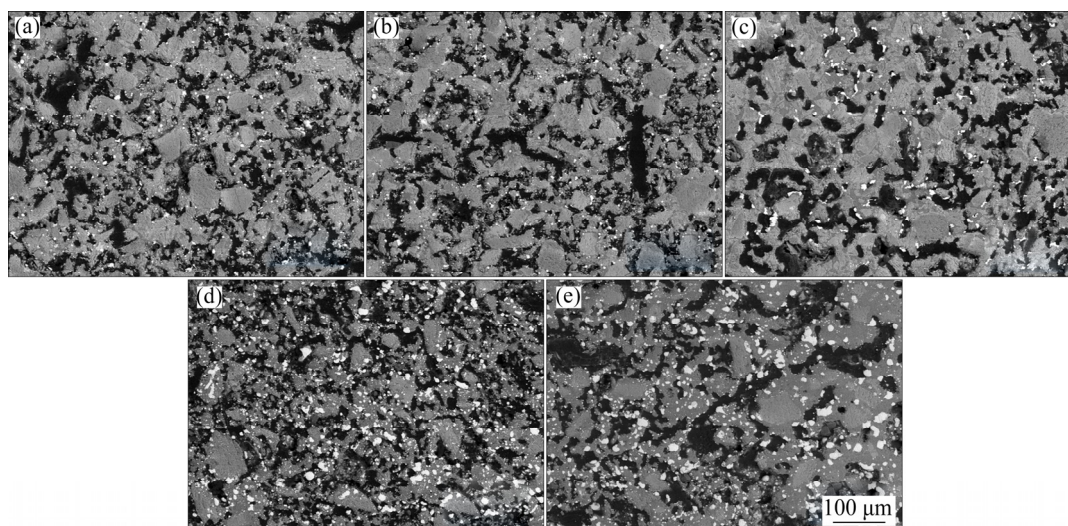


**Fig. 7** SEM images of nickel slag added with different contents of  $\text{CaCO}_3$  reduced at 1100 °C: (a) 0 wt.%; (b) 2 wt.%; (c) 4 wt.%; (d) 6 wt.%; (e) 8 wt.%

As the added  $\text{CaCO}_3$  content increased, the amounts of iron particles increased (bright white areas) and their size was coarsened. The sizes of the iron particles shown in Figs. 7(a) and 7(e) were measured using Image-Pro Plus software. The results showed that the average size of the iron particles was  $6 \mu\text{m}$  after reduction of the slag without adding  $\text{CaCO}_3$ , but increased to  $21 \mu\text{m}$  when 6 wt.%  $\text{CaCO}_3$  was added. The structure of the product without the  $\text{CaCO}_3$  was compact, which made its growth and accumulation difficult; by adding  $\text{CaCO}_3$ , cracks and pores formed during the reaction, which provided channels for the reducing gas and accelerated the reduction process.

XRD patterns of the nickel slag added with different contents of  $\text{CaCO}_3$  reduced at  $1100^\circ\text{C}$  are shown in Fig. 8. The peak intensities of  $\text{Fe}_2\text{SiO}_4$  decreased as the  $\text{CaCO}_3$  content increased, due to its reaction with Mg and CaO to form  $\text{Mg}_2\text{SiO}_4$  and Fe. As a result, the peak intensity of  $\text{Mg}_2\text{SiO}_4$  and Fe gradually increased and that of  $\text{CaFeSi}_2\text{O}_6$  decreased. The chemical reactions are as follows:



### 3.2.2 Effect of temperature

SEM images and EDS data of the nickel slag added with 8 wt.%  $\text{CaCO}_3$  reduced at different temperatures are shown in Fig. 9 and Table 3, respectively. The SEM images showed that only few iron grains (bright white areas) were observed at 600 and 800  $^\circ\text{C}$ . The amount and size of the iron grains increased with the temperature increasing. The structure of the product was relatively

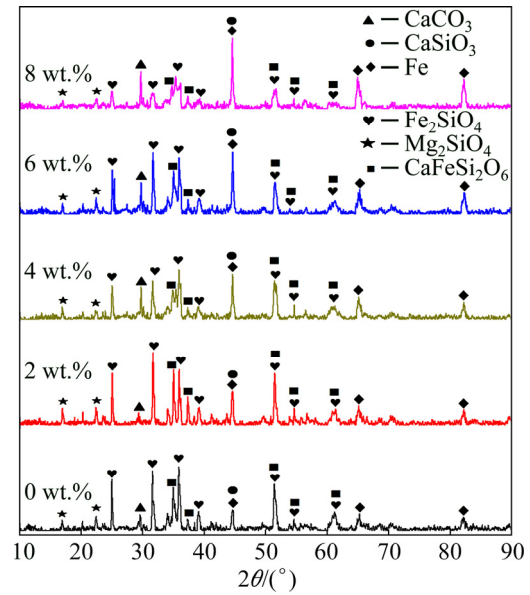


Fig. 8 X-ray diffraction patterns of nickel slag added with different contents of  $\text{CaCO}_3$  reduced at  $1100^\circ\text{C}$

loose at low temperature and became denser with the increase of temperature.

The results of the EDS analysis in Table 3 showed that the reduced samples were composed of Fe, Mg, Si, Ca, C, O and a small amount of S. Iron present in the whole region, but calcium, magnesium, silicon and oxygen only present in the slag phase.

XRD patterns of the reduced products at different temperatures are shown in Fig. 10.

At 600  $^\circ\text{C}$ , the intensities of the  $\text{CaCO}_3$  diffraction peaks were higher than those at other temperatures because no decomposition occurred at this temperature;

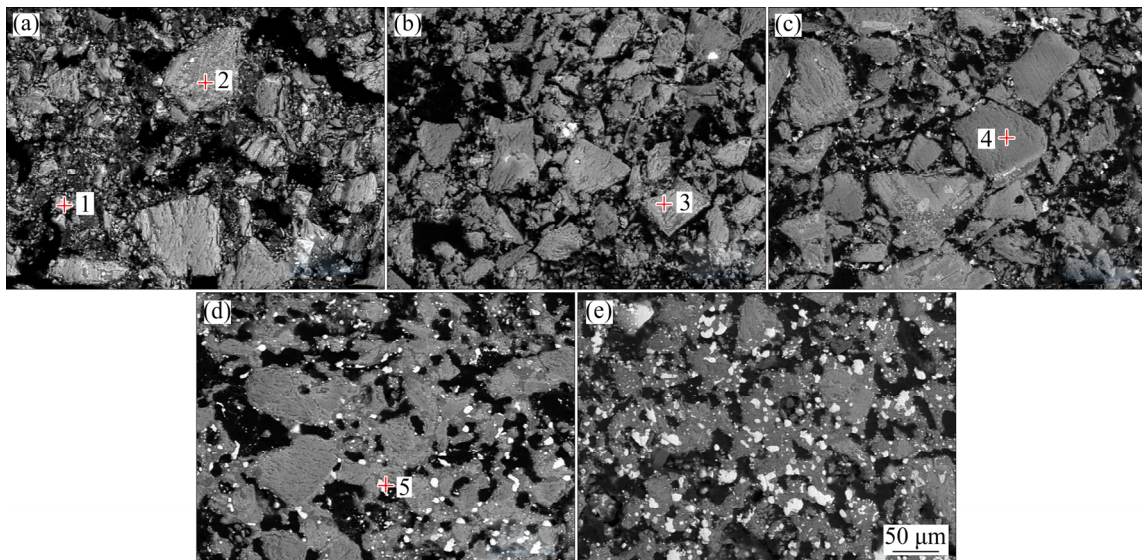


Fig. 9 SEM images of reduced nickel slag added with 8 wt.%  $\text{CaCO}_3$  at different temperatures: (a)  $600^\circ\text{C}$ ; (b)  $800^\circ\text{C}$ ; (c)  $1000^\circ\text{C}$ ; (d)  $1100^\circ\text{C}$ ; (e)  $1200^\circ\text{C}$

the diffraction peak intensities decreased at 800 °C because some  $\text{CaCO}_3$  was decomposed. The main chemical reaction is expressed by



**Table 3** EDS data of nickel slag added with 8 wt.%  $\text{CaCO}_3$  at different temperatures

Point in Fig. 9	Content/wt.%						
	O	Mg	Si	Ca	Fe	C	S
1	37.28	10.02	15.32	—	33.55	3.83	2.71
2	39.27	0.79	3.36	28.98	8.16	17.31	—
3	45.70	—	23.28	6.90	14.60	—	0.44
4	38.20	0.78	19.01	11.98	23.36	2.48	1.56
5	—	—	1.22	—	95.36	1.83	—

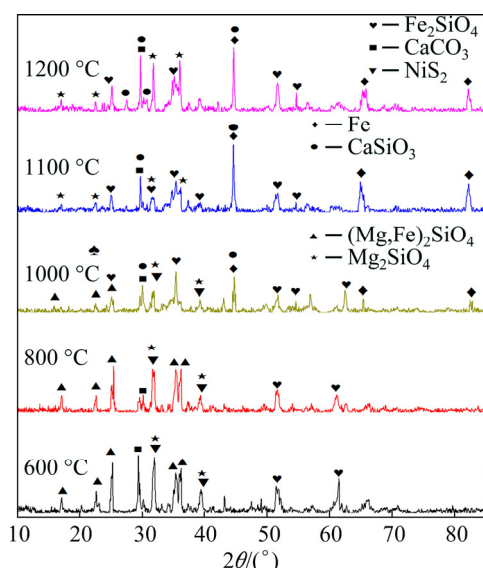


**Fig. 10** X-ray diffraction patterns of reduced products with 8 wt.%  $\text{CaCO}_3$  at different temperatures

As the reaction temperature increased, the structure of slag gradually changed from amorphous to crystalline and iron appeared as a result of the reaction of fayalite with  $\text{CaO}$  and carbon. The main chemical reaction is given by



$\text{Fe}$  diffraction peaks appeared at 1000 °C. As the temperature increased, the intensity of the diffraction peaks of  $\text{Fe}_2\text{SiO}_4$  gradually decreased and diffraction peaks of  $\text{CaSiO}_3$  began to appear.  $(\text{Mg},\text{Fe})_2\text{SiO}_4$  gradually disappeared as the temperature increased, which was mainly due to the reaction between  $\text{MgO}$  and  $\text{Fe}_2\text{SiO}_4$  to form  $\text{Mg}_2\text{SiO}_4$ . The main chemical reaction is expressed by



#### 4 Mechanism analysis

XRD analysis showed that  $\text{Fe}$  in the sample present as  $\text{Fe}_2\text{SiO}_4$  primarily. During reduction,  $\text{C}$  had difficulty in directly reacting with fayalite. After adding  $\text{CaCO}_3$ , the  $\text{Ca}^{2+}$  ions were used as the carrier of  $\text{SiO}_4^{2-}$  in olivine. The proposed reaction mechanism is shown in Fig. 11.

When  $\text{CaCO}_3$  came into contact with  $\text{Fe}_2\text{SiO}_4$ , the presence of  $\text{Ca}^{2+}$  weakened the bond between  $\text{SiO}_4^{2-}$  and  $\text{Fe}^{2+}$ . Since the binding abilities of  $\text{Ca}^{2+}$  and  $\text{SiO}_4^{2-}$  were strong, the chemical bond was broken under reducing conditions to form  $\text{FeO}$  and  $\text{Ca}_2\text{SiO}_4$ .  $\text{FeO}$  was further reduced to iron by the carbon added to the nickel slag. The main chemical reactions are expressed by

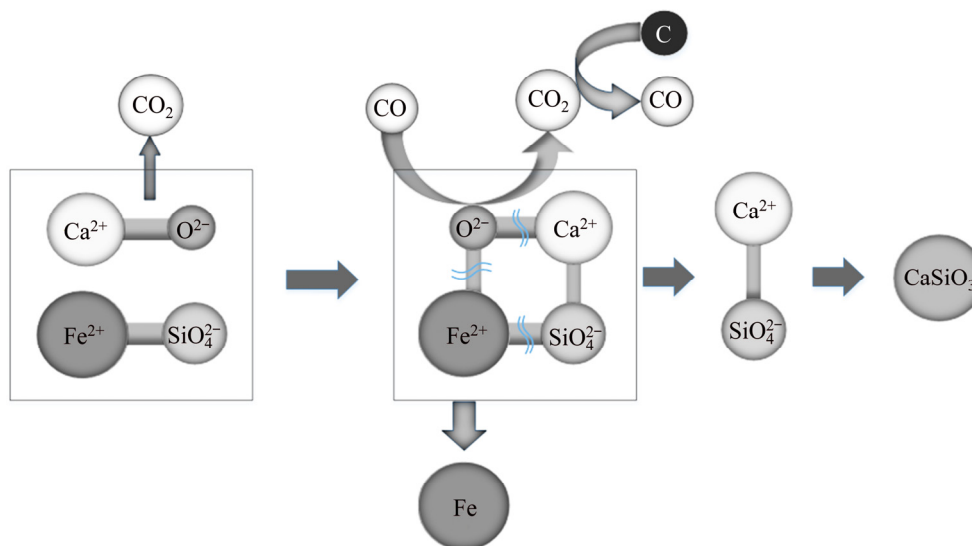


**Fig. 11** Mechanism of acceleration of iron reduction from nickel slag by  $\text{CaCO}_3$

It is worth noting that when the reaction temperature was high, the nickel slag underwent some sintering during reduction and the reduced FeO combined with SiO<sub>2</sub> to form liquid-phase FeO·SiO<sub>2</sub>, which seriously deteriorated the reduction kinetics and hindered the reduction reaction [19]. The CaO activity generated by pyrolysis of CaCO<sub>3</sub> was high and the binding ability of CaO and SiO<sub>2</sub> was stronger than that of FeO. CaO combined with SiO<sub>2</sub> to form CaO·SiO<sub>2</sub>, which hindered the formation of liquid-phase FeO·SiO<sub>2</sub> and improved the reduction conditions. As the reduction reaction proceeded, the resulting slag phase hindered the contact of the carbon with iron oxide to a certain extent and the chemical reaction transformed to a gas-based reaction. CO<sub>2</sub> generated by the decomposition of CaCO<sub>3</sub> at high temperatures accelerated the melting loss of carbon [20] and the reduction reaction increased the CO content of the gaseous reductant, thereby improving the reduction of nickel slag.

Previous studies have shown that the amount of CaCO<sub>3</sub> added is limited. The reason is that CaCO<sub>3</sub> will decompose to produce CaO at high temperature, which affects the basicity and melting point of the slag.

The phase diagram of the CaO–SiO<sub>2</sub>–MgO system is shown in Fig. 12. When the contents of SiO<sub>2</sub> and MgO are constant and a small amount of CaCO<sub>3</sub> is added, the calcium oxide content and basicity of the nickel slag are lower. The melting point of the slag is higher under low-basicity conditions. As the added CaCO<sub>3</sub> content increases, the basicity of the sample gradually increases. This decreases the melting point of the slag and more slag will melt during the reduction process [21,22]. The impurity of the sample increases, which would affect the reduction process to some extent. Molten slag blocks the porosity of the sample, which decreases the porosity of the nickel slag and hinders the reduction.

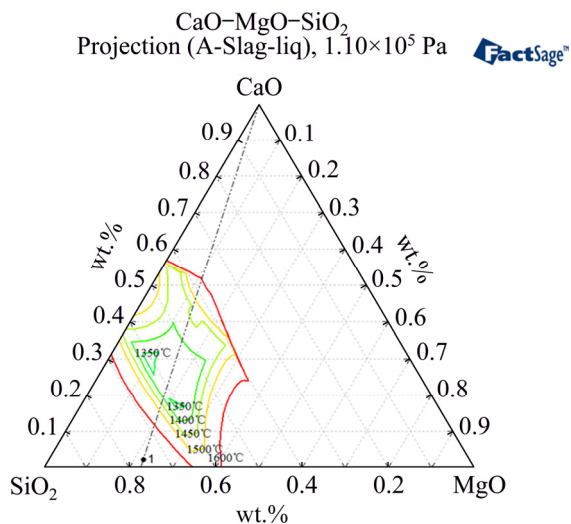


Fig. 12 Phase diagram of CaO–SiO<sub>2</sub>–MgO system

## 5 Conclusions

(1) Adding CaCO<sub>3</sub> increased the reaction rate and decreased the temperature of the reduction reaction. Carbothermic reduction of nickel slag began at 1000 °C. The higher the temperature, the larger the reaction rate was. In the absence of CaCO<sub>3</sub>, the reduction rate reached a maximum of 0.143 mg/min between 1100 and 1150 °C. When the CaCO<sub>3</sub> content was increased to 8 wt.%, the initial temperature of carbothermic reduction reaction of nickel slag was reduced to 1000 °C, and the temperature reaching the maximum reaction rate was reduced to 1100 °C.

(2) After 90 min reduction, the reduction degree of iron in the sample without adding CaCO<sub>3</sub> was 58%. The reduction degree of iron increased to 70%, 80%, 85% and 88% when the added CaCO<sub>3</sub> content was 2, 4, 6 and 8 wt.%, respectively, which indicated that CaCO<sub>3</sub> had a positive effect on the reduction of nickel slag.

(3) The average size of the iron particles in reduced nickel slag without adding CaCO<sub>3</sub> was 6 μm, but increased to 21 μm when 6 wt.% CaCO<sub>3</sub> was added.

(4) A feasible process to recover iron from nickel slag by carbothermic reduction was proposed. The optimum parameters were 8 wt.% CaCO<sub>3</sub> added, reduction temperature 1200 °C, and reduction time 45 min.

## References

- [1] ZHANG Chuan-fu, LIU Hai-xia, ZHONG Da-long. Thermodynamical analysis of smelting process of nickel sulfides concentrate [J]. The Chinese Journal of Nonferrous Metals, 1999, 9: 805–810. (in Chinese)
- [2] LI Xiao-ming, SHEN Miao, WANG Chong, CUI Ya-ru, ZHAO Jun-xue. Current situation and development of comprehensive utilization of nickel slag [J]. Materials Review, 2017, 31(5): 100–105. (in Chinese)
- [3] PIATAK N M, PARSONS M B, SEAL R R. Characteristics and environmental aspects of slag: A review [J]. Applied Geochemistry, 2015, 57: 236–266.
- [4] CHEN Wei-peng, LI Guang-wei, ZHAO Zeng-wu, LI Bao-wei, WU Wen-fei. Direct reduction of limonite with iron-rich coal slime as reducing agent [J]. Mining and Metallurgical Engineering, 2017, 37(1): 68–72. (in Chinese)
- [5] PANG Jian-ming, GUO Pei-min, ZHAO Pei. New technology of low-temperature reduction and grain growth of copper slag [J]. Non-ferrous Metals (Extractive Metallurgy), 2013(3): 51–53, 57. (in Chinese)
- [6] ZHAO Zhi-long, TANG Hui-qing, GUO Zhan-cheng. Influences of CaO and MgO on precipitation micro-morphology of metallic iron under CO atmosphere [J]. Mining and Metallurgical Engineering, 2012, 32(5): 105–109, 112. (in Chinese)
- [7] BAI Shao-jun, WEN Shu-ming, LIU Dian-wen, ZHANG Wen-bin, CAO Qin-bo. Beneficiation of high phosphorus limonite ore by sodium-carbonate-added carbothermic reduction [J]. ISIJ International, 2012, 52(10): 1757–1763.

- [8] BAI Shao-jun, WEN Shu-ming, LIU Dian-wen, ZHANG Wen-bin, XIAN Yong-jun. Catalyzing carbothermic reduction of siderite ore with high content of phosphorus by adding sodium carbonate [J]. ISIJ International, 2011, 51(10): 1601–1607.
- [9] DING Shan, XUE Qing-guo, SHE Xue-feng, WANG Guang, NING Xiao-yu, WANG Jing-song. Effect of  $\text{CaCO}_3$  on direct reduction-smelting separation of vanadium-bearing titanomagnetite concentrate [J]. Iron and Steel, 2014, 49(8): 15–20. (in Chinese)
- [10] KIM H, SOHN I. Effect of  $\text{CaF}_2$  and  $\text{Li}_2\text{O}$  additives on the viscosity of  $\text{CaO-SiO}_2\text{-Na}_2\text{O}$  slags [J]. ISIJ International, 2011, 51: 1–8.
- [11] KIM H, MATSUURA H, TSUKIHASHI F. Effect of  $\text{Al}_2\text{O}_3$  and  $\text{CaO/SiO}_2$  on the viscosity of calcium-silicate-based slags containing 10 mass Pct MgO [J]. Metall Mater Trans B, 2013, 44: 5–12.
- [12] BASUMALLICK A. Influence of  $\text{CaO}$  and  $\text{Na}_2\text{CO}_3$  as additive on the reduction of hematite-lignite mixed pellets [J]. Transactions of the Iron & Steel Institute of Japan, 2007, 35(9): 1050–1053.
- [13] XU Yan, SUN Ti-chang, LIU Zhi-guo, XU Cheng-yan. Dephosphorization effects of sodium carbonate in the process of direct reduction roasting of high phosphorous oolitic hematite [J]. Journal of Northeastern University (Natural Science Edition), 2014, 35(7): 1028–1032. (in Chinese)
- [14] SUN Yong-sheng, HAN Yue-xin, GAO Peng, WEI Xin-chao, LI Guo-feng. Thermogravimetric study of coal-based reduction of oolitic iron ore: Kinetics and mechanisms [J]. International Journal of Mineral Processing, 2015, 143: 87–97.
- [15] CAO Yu-xin, WANG Heng-hui, MA Jiang-hua, ZHAO Dong, LI Guang-qiang. Effect of additives on the preparation of reduced iron powder from iron concentrate [J]. The Chinese Journal of Process Engineering, 2018, 18(1): 133–139. (in Chinese)
- [16] LI Guang-hui, ZHOU Tai-hua, LIU Mu-dan, JIANG Tao, FAN Xiao-hui. Novel process and mechanisms of aluminum-iron separation of high-aluminum limonite ore [J]. The Chinese Journal of Nonferrous Metals, 2008, 18: 2087–2093. (in Chinese)
- [17] JIANG Tao, LIU Mu-dan, LI Guang-Hui, SUN Na, ZENG Jing-hua, QIU Guang-zhou. Novel process for treatment of high-aluminum limonite ore by reduction roasting with addition of sodium salts [J]. The Chinese Journal of Nonferrous Metals, 2010, 20: 565–571. (in Chinese)
- [18] HUANG Bin-fang, LIU Bin, YANG Lei, LI Y, CHENG M, HUANG D, WANG H, ZHANG X, ZHENG J, LI Q, JI W, ZHOU Y, LU J. Functional genetic variants of *c-Jun* and their interaction with smoking and drinking increase the susceptibility to lung cancer in southern and eastern Chinese [J]. International Journal of Cancer, 2012, 131(5): E744–E758.
- [19] ZHANG Jian-liang, WANG Chun-long, LIU Zheng-jian, WANG Zhe, CAO Ming-ming. Influencing factors of the reduction of vanadium titano-magnetite carbon composite pellets [J]. Journal of University of Science and Technology Beijing, 2012, 34(5): 512–518. (in Chinese)
- [20] AN Xiu-wei, WANG Jing-song, SHE Xue-feng, DING Yin-gui, XU Qing-guo. New technologies of energy saving and low  $\text{CO}_2$  emission for iron making [J]. Advanced Materials Research, 2012, 463–464: 957–961.
- [21] YU Hai-yan, PAN Xiao-lin, DONG Kai-wei, WU Yan. Effect of P addition on mineral transition of  $\text{CaO-Al}_2\text{O}_3\text{-SiO}_2$  system during high-temperature sintering [J]. Transactions of Nonferrous Metals Society of China, 2019, 29(3): 650–656.
- [22] YU Wen-zhou, MA Wen-hui, ZHENG Zhong, JIANG Wei-yan, LI Jie, Mao-hong TIAN. Effects of melt viscosity on enrichment and separation of primary silicon from Al-Si melt [J]. Transactions of Nonferrous Metals Society of China, 2017, 27(2): 467–474.

## 添加碳酸钙促进镍渣碳热还原

李小明<sup>1,2</sup>, 闻震宇<sup>1</sup>, 李怡<sup>1</sup>, 杨海博<sup>1</sup>, 邢相栋<sup>1,2</sup>

1. 西安建筑科技大学 冶金工程学院, 西安 710055;

2. 西安建筑科技大学 陕西省冶金工程技术研究中心, 西安 710055

**摘要:** 研究添加碳酸钙对镍渣碳热还原过程的影响, 并分析其机理。结果表明, 随着原料中碳酸钙添加量从 0 增加到 8%(质量分数), 还原反应初始温度和达到最大反应速率所需的温度分别从 1100 和 1150 °C 降低到 1000 和 1100 °C, 镍渣的还原率从 58%增加到 88%; 还原后的渣中铁粒发生粗化, 金属铁的衍射峰强度增加, 表明添加碳酸钙有利于促进镍渣中铁化合物的还原回收。

**关键词:** 镍渣; 铁橄榄石; 碳热还原; 碳酸钙

(Edited by Bing YANG)